JOURNAL OF MAGNETIC RESONANCE 94, 82–100 (1991)

2D Heteronuclear NMR Measurements of Spin–Lattice Relaxation Times in the Rotating Frame of X Nuclei in Heteronuclear HX Spin Systems

JEFFREY W. PENG,*† V. THANABAL,* AND GERHARD WAGNER*‡

*Department of Biological Chemistry and Molecular Pharmacology, Harvard Medical School, 240 Longwood Avenue, Boston, Massachusetts 02115; and †Biophysics Research Division, University of Michigan, 2200 Bonisteel Boulevard, Ann Arbor, Michigan 48109

Received November 30, 1990

Theoretical and experimental aspects of $T_{1\rho}$ are discussed for a heteronuclear HX two-spin system ($T_{1\rho}^X$) where only the X nucleus is spin-locked. An expression for $T_{1\rho}^X$ in terms of spectral density functions and the effective magnetic field parameters is developed. It shows that $T_{1\rho}^X$ offers potentially different information about the spectral densities than either T_1^X, T_2^X, or the steady-state NOE^X. We present a 2D heteronuclear NMR pulse sequence for measuring site-specific $T_{1\rho}^X$'s in biomolecules. The sequence is based on a double-INEPT transfer and applies a spin lock to the heteronuclei for variable delays. If a weak on-resonance spin lock is used, and if the spectral density functions are assumed to be Lorentzians, then $T_{1\rho}^X$ is theoretically indistinguishable from T_2^X. We conclude with an application of the pulse sequence to the uniformly ^{15}N-enriched protein eglin c. The $T_{1\rho}^X$ data reflect the differential mobility in the molecule.

NMR relaxation studies of X nuclei in heteronuclear HX spin systems can provide information about the global and internal motions of biomolecules (*1–3*). Hence, they are powerful tools for the experimentalist interested in biomolecular dynamics. Recently developed techniques for measuring such relaxation times use various heteronuclear multidimensional NMR pulse sequences to provide the necessary frequency resolution, as well as to lend sensitivity enhancement (*1, 3*). Additionally, the increasing availability of isotopic enrichment alleviates the problem of poor sensitivity due to low natural abundance of such biological heteronuclei as ^{15}N and ^{13}C. Making use of these assets, dynamical information for a large number of different sites in the molecule can simultaneously be obtained.

Thus far the most commonly measured relaxation parameters of heteronuclei HX spin systems include T_1^X, T_2^X, and the steady-state NOE^X that develops due to saturation of the H spin (*1–3*). In this paper, we discuss the measurement of the spin–lattice relaxation time in the rotating frame, $T_{1\rho}^X$. $T_{1\rho}^X$ is the decay constant of magnetization locked along the effective field, $\mathbf{B}_{\text{eff}}$. Previous studies of $T_{1\rho}$ include work by Abragam (*4*), Jones (*5*), James (*6–9*), and Blicharski (*10a, 10b*). The derivation of the homonuclear $T_{1\rho}$ has been given by Jones (*5*) and Blicharski (*10a, 10b*). James *et al.* (*6, 9*) have used 1D ^{13}C off-resonance $T_{1\rho}^X$ measurements to get information about protein rotational correlation times and internal dynamics.

‡ To whom correspondence should be addressed.

0022-2364/91 $3.00

In this paper, we use the semiclassical relaxation formalism to arrive at an expression for $T_{1\rho}^{X}$ for an HX spin system. Our approach follows that of Jones (*5*). $T_{1\rho}^{X}$ is expressed in terms of the spectral density functions, $J(\omega)$, and the radiofrequency flip angle, β. An expression is also obtained for the heteronuclear cross-relaxation rate in the rotating frame, σ_{ρ}^{HX}. Blicharski (*10a*) has given a $T_{1\rho}^{X}$ expression in terms of the Wigner 3-j symbols, assuming isotropic rigid tumbling of the molecule. If we assume rigid body tumbling of the molecule as well, then our results are equivalent to that contained in the more general expression of Blicharski (*10a*). We also present a 2D NMR pulse sequence to measure $T_{1\rho}^{X}$ for each heteronucleus in the molecule of interest. We then present $T_{1\rho}^{X}$ relaxation data from the proteinase inhibitor eglin c 100% isotopically enriched in ^{15}N.

Relaxation parameters are related to overall and internal molecular motions through their dependence on the spectral density functions, $J(\omega)$. Specifically, the relaxation parameters sample the spectral density at particular frequencies with varying weights. It is seen that $T_{1\rho}^{X}$ samples different frequencies of $J(\omega)$ than either T_1^X, T_2^X, or the steady-state NOE^X. In principle, this means that $T_{1\rho}^{X}$ can give new information concerning the spectral properties of $J(\omega)$. The $T_{1\rho}^{X}$ data on eglin c support the information from other relaxation parameter measurements (T_1^X, NOE^X) in revealing the more mobile regions of the molecule. Thus, $T_{1\rho}^{X}$ is sensitive to dynamical heterogeneity in biomolecules.

THEORY

$T_{1\rho}^{X}$ is the relaxation time for magnetization along the effective magnetic field in the rotating frame. The physical situation is illustrated for an arbitrary spin-$\frac{1}{2}$ nucleus with Larmor frequency ω_0 in Fig. 1. The rotating frame is defined by the xyz axes, with the static, superconducting field $\mathbf{B}_0$ pointing along $+z$. $\mathbf{B}_0$ defines the laboratory Z axis, which is coincident with the rotating-frame z axis. The effective field is indicated by the vector $\mathbf{B}_{eff}$, which is tipped away from the z axis by an angle β. The z component

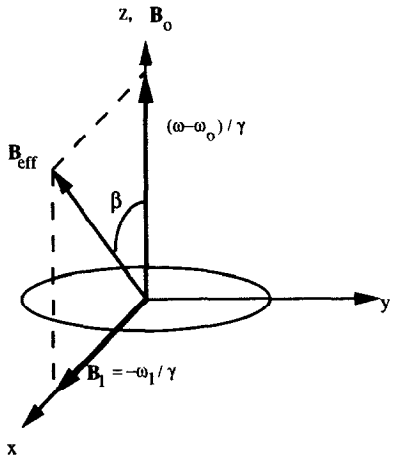

FIG. 1. Magnetic field vectors in the rotating frame for a nucleus of Larmor frequency ω_0.

of $\mathbf{B}_{\text{eff}}$ is $(\omega - \omega_0)/\gamma$ and is proportional to the detuning of the applied RF field frequency ω, from the resonance frequency ω_0. The x component is the applied RF spin-lock field, $\mathbf{B}_1$, where $\omega_1 = -\gamma B_1$. Thus, the magnitude and tip angle β of $\mathbf{B}_{\text{eff}}$ are parameterized in terms of ω, ω_1 in the usual way as

$$\tan(\beta) = \frac{\gamma B_1}{(\omega - \omega_0)} = \frac{\omega_1}{(\omega_0 - \omega)}$$

$$B_{\text{eff}} = \frac{1}{\gamma}\sqrt{\omega_1^2 + (\omega - \omega_0)^2} = -\frac{\omega_e}{\gamma}, \qquad [1]$$

where ω_e is the effective field described in angular frequency units. When $\beta = (\pi/2)$, $\mathbf{B}_{\text{eff}}$ becomes identical to $\mathbf{B}_1$; this corresponds to the resonance condition $\omega = \omega_0$. In the absence of any RF fields, all applied fields vanish in the rotating frame. Only local perturbing fields remain, and therefore this constitutes an interaction frame in which the relaxation analysis for T_1 and T_2 can be done (*4, 11*).

Extraction of an expression for $T_{1\rho}^{X}$ in a heteronuclear HX spin system requires the following steps. We first define the Hamiltonian operator for two unlike spins in the laboratory frame. We must then perform a rotation transformation of the Hamiltonian, so that we can work in an interaction frame where the applied fields have vanished. Note that we have two applied fields: the static $\mathbf{B}_0$ and the radiofrequency spin-lock field $\mathbf{B}_1$. Therefore, we need to transform to a *doubly* rotating frame. After this, only terms concerning the local perturbing fields remain. We can then use semiclassical relaxation theory to get a rate equation for the decay of magnetization along $\mathbf{B}_{\text{eff}}$. The resulting rate constant is $1/T_{1\rho}^{X}$. The use of operator methods as discussed by Abragam obviates the need to solve explicitly for the spin density matrix, $\sigma(t)$, as a function of time. This is discussed thoroughly by Abragam (*4*) and Ernst *et al.* (*11*).

Laboratory Hamiltonian. We consider an ensemble of HX spin systems subject to three magnetic fields: the static field $\mathbf{B}_0$, the applied RF spin-lock field on the X nuclei at radial frequency ω, and the local perturbing fields from the non-spin–lattice processes. Examples of such spin systems are the backbone amide nitrogens and their directly bonded protons in proteins. Since our analysis is applied to such real spin systems, we hereafter refer to the HX spins as the amide protons and their ^{15}N nuclei.

The spin-Hamiltonian operator $\mathscr{H}$ gives the magnetic energy of the ^{1}H–^{15}N system in terms of both spin product operators and magnetic field parameters. Generally, the latter may be functions of time. The three fields allow $\mathscr{H}$ to be partitioned conveniently as

$$\mathscr{H} = \mathscr{H}_Z + \mathscr{H}_{RF} + V(t). \qquad [2]$$

$\mathscr{H}_Z$ is the Zeeman energy contribution from $\mathbf{B}_0$ and is given by

$$\mathscr{H}_Z = \omega_p I_z + \omega_n N_z, \qquad [3]$$

where ω_n and ω_p are the Larmor frequencies for the ^{15}N nucleus and the amide proton, respectively. Note that we have expressed the Hamiltonian in units of $h/2\pi$. I_z and N_z are the associated proton and ^{15}N z-magnetization spin operators and are part of a 16-dimensional product-operator basis (*12*).

$\mathcal{H}_{RF}$ is the spin-lock-RF-field ($\mathbf{B}_1$) contribution and is written as

$$\mathcal{H}_{RF} = \omega_1[\cos(\omega t)N_x + \sin(\omega t)N_y]. \quad [4]$$

This expression indicates that the RF field oscillates at a radial frequency of ω and operates only on the ^{15}N nuclei (for an 11.74 T magnet $\omega_n/2\pi \approx 50.68$ MHz). In the rotating frame, the RF field is simply a static field along the x axis.

$V(t)$ is the perturbing operator in the Hamiltonian and contains the effects of the local fluctuating magnetic fields. In general, $V(t)$ can be expressed as a sum of products of spin operators $A^{(q)}$ and temporal functions associated with the lattice (nonspin) degrees of freedom, $F^{(q)}(t)$. It is written as

$$V(t) = \sum_{q=-M}^{M} F^{(q)}(t)A^{(q)}. \quad [5]$$

Thus, $V(t)$ couples the spin and lattice degrees of freedom of the nuclei. For a given integer M, there are $2M + 1$ terms. However, since $V(t)$ must be a Hermitian operator we need to specify only $M + 1$ terms. The other M are fixed by the Hermitian conjugation relations

$$A^{(q)\dagger} = A^{(-q)}$$
$$F^{(q)*} = F^{(-q)}. \quad [6]$$

The dagger indicates Hermitian conjugation while the asterisk indicates complex conjugation. Equation [5] shows that the temporal behavior of $V(t)$ is dictated by the $F^{(q)}(t)$ functions. The $F^{(q)}(t)$ are assumed to have stochastic behavior with an average value of 0. Their explicit form is

$$F^{(q)}(\theta(t), \phi(t)) = C^{(q)}Y_{2,-q}(\theta(t), \phi(t)). \quad [7]$$

The $Y_{2,-q}(\theta(t), \phi(t))$ are the second-order spherical harmonics, and the $C^{(q)}$ are real constants that depend on the index q.

In general, a variety of sources can give rise to fluctuating fields. An example is the local dipolar field of a closely neighboring spin that is in relative motion with respect to the spin of interest. Another example is the reorientation of a given spin's own anisotropic chemical-shift tensor. Each source will contribute a perturbation, $V(t)$, of the form given in Eq. [5]. Here, we focus on perturbations due to the local dipole–dipole interactions between a pair of unlike spins. The interaction is a primary relaxation mechanism in typical HX relaxation studies of biomolecules. For this interaction, $M = 2$ in Eq. [5]. The spin operators for $q = 0, 1, 2$ are

$$A^{(0)} = I_zN_z - \tfrac{1}{4}(I_+N_- + I_-N_+)$$
$$A^{(1)} = I_zN_+ + I_+N_z$$
$$A^{(2)} = I_+N_+, \quad [8]$$

where $I_\pm = I_x \pm iI_y$ and $N_\pm = N_x \pm iN_y$. Spin operators for $q = -1, -2$ are found by using the Hermiticity relations in Eq. [6]. The operators connect spin states that differ by q in the total magnetic quantum number. The corresponding lattice functions $F^{(q)}(\theta(t), \phi(t))$ are given as

$$F^{(0)} = \alpha \sqrt{\frac{16\pi}{5}}\, Y_{2,0}(\theta(t), \phi(t))$$

$$F^{(1)} = \frac{3\alpha}{2} \sqrt{\frac{8\pi}{15}}\, Y_{2,-1}(\theta(t), \phi(t))$$

$$F^{(2)} = \frac{3\alpha}{4} \sqrt{\frac{32\pi}{15}}\, Y_{2,-2}(\theta(t), \phi(t)), \quad [9]$$

where $\alpha = \gamma_n\gamma_p/r_{np}^3$.

The variables $\theta(t)$ and $\phi(t)$ describe the orientation of the ^{15}N–H bond vector $\mathbf{r}_{np}(t)$, with respect to the static field $\mathbf{B}_0$. The vector undergoes rotational diffusion due to the overall tumbling of the molecule and any internal dynamics, while the spin degrees of freedom stay parallel or antiparallel with $\mathbf{B}_0$. In this way, the $F^{(q)}$ become stochastic functions of time. In summary the net perturbation operator of the laboratory Hamiltonian due to dipole–dipole interactions is

$$V(t) = -\alpha(3\cos^2\theta - 1)\left(I_zN_z - \frac{1}{4}(I_+N_- + I_-N_+)\right)$$
$$- \frac{3\alpha}{2}[\sin\theta\cos\theta(e^{-i\phi})](I_zN_+ + I_+N_z) + \text{HC}$$
$$- \frac{3\alpha}{4}[\sin^2\theta(e^{-i2\phi})](I_+N_+) + \text{HC}, \quad [10]$$

where HC indicates the Hermitian conjugate of the preceding term.

Transformation to the doubly rotating coordinate frame. We are now in a position to change to an interaction frame wherein the applied field terms in the Hamiltonian vanish. Note that the traditional rotating frame will not suffice since it retains the effective field, $\mathbf{B}_{eff}$. A convenient approach is given by Abragam (*4*). In this approach we transform the Hamiltonian to a doubly rotating frame. This frame is the result of three successive rotation transformations on the laboratory coordinate frame. Therefore, these rotations are best described by the Euler angles α, β, and γ. The first rotation is through an angle $\alpha(t) = \omega t$ about the laboratory Z axis. We show this in Fig. 2a. Uppercase labels X, Y, and Z mark the laboratory axes and lowercase labels x, y, and z mark the rotated axes. The result is the usual rotating frame, as in Fig. 1. We continue with a second rotation through the angle β about the new y axis (line of nodes), as shown in Fig. 2b. This results in the axes x^*, y^*, and z^*. The angle β is the same tip angle for the effective field $\mathbf{B}_{eff}$ as that shown in Fig. 1. Therefore, the z^* axis is parallel to $\mathbf{B}_{eff}$. From the perspective of a spectroscopist in the $x^*y^*z^*$ frame, $\mathbf{B}_{eff}$ serves the same purpose as $\mathbf{B}_0$ did in the laboratory frame. Thus, it can be "transformed away" in the same manner that $\mathbf{B}_0$ was. Namely, we do a third rotation through an angle $\gamma(t) = \omega_e t$ about the tipped z^* axis (figure axis). This brings us to the final coordinate frame $x'y'z'$, where z' and z^* are the same. This last rotation is shown in Fig. 2c. All applied magnetic fields have vanished; thus, we have transformed to the interaction frame appropriate for the study of relaxation phenomena of the simpler *rotating* frame.

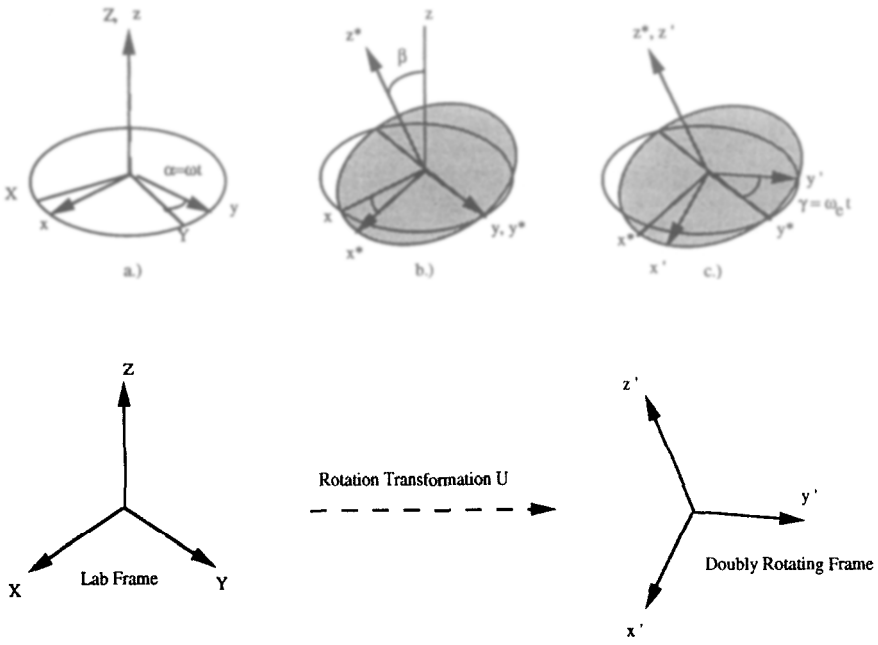

FIG. 2. The three successive rotations of the doubly rotating frame. (a) Rotation about laboratory Z axis through $\alpha = \omega t$. (b) Rotation about y (line of nodes) through tip angle β. Effective field $\mathbf{B}_{\text{eff}}$ is parallel to z^*. (c) Final rotation about z^* (figure axis) through $\gamma = \omega_c t$. Below, the laboratory axes are denoted by the XYZ axes, and the doubly rotating frame axes are denoted by the $x'y'z'$ axes.

Since the proton spin operators commute with the nitrogen spin operators, the proton rotation transformations can be considered independently. In particular, whereas three rotations were necessary for the ^{15}N nuclei (X nuclei), only one is necessary for the protons (^{1}H nuclei) since the latter suffer no spin lock. Thus the required proton rotation transformation is about the laboratory Z axis through an angle $\alpha = \omega_p t$. The total rotation transformation is then given by the unitary operator U, which consists of the three ^{15}N rotations and the single proton rotation. It is written as

$$U = U_p U_n, \qquad [11a]$$

where

$$U_p = \exp(i\omega_p t I_z) \qquad [11b]$$

and

$$U_n = \exp(i\omega_c t N_z)\exp(i\beta N_y)\exp(i\omega t N_z). \qquad [11c]$$

Of course, since the nitrogen and proton spin operators commute, the order of transformation in Eq. [11a] is irrelevant.

To summarize, the effective Hamiltonian in the doubly rotating frame is obtained by applying the net rotation operator U to the laboratory expression given in Eq. [2].

The end result is simply the rotated version of $V(t)$. We designate this transformed operator as $V'(t)$. In terms of the spin operators and lattice functions, we have

$$V'(t) = UV(t)U^{\dagger}$$

$$\begin{aligned}
&= -\alpha \sqrt{\frac{16\pi}{5}}\, Y_{2,0}(\theta(t), \phi(t))\Big\{cI_zN'_z - (s/2)e^{i\omega_e t}I_zN'_+ + \mathrm{HC} \\
&\quad - \frac{1}{4}((c-1)/2)e^{i(\omega_p-\omega_n+\omega_e)t}I_+N'_+ + \mathrm{HC} \\
&\quad - \frac{1}{4}se^{i(\omega_p-\omega_n)t}I_+N'_z + \mathrm{HC} \\
&\quad - \frac{1}{4}((c+1)/2)e^{i(\omega_p-\omega_n-\omega_e)t}I_+N'_- + \mathrm{HC}\Big\} \\
&\quad - \frac{3\alpha}{2} \sqrt{\frac{8\pi}{15}}\, Y_{2,-1}(\theta(t), \phi(t))\{(c+1)/2)e^{i(\omega_n+\omega_e)t}I_zN'_+ \\
&\quad + se^{i\omega_n t}I_zN'_z + ((c-1)/2)e^{i(\omega_n-\omega_e)t}I_zN'_- - (s/2)e^{i(\omega_p+\omega_e)t}I_+N'_+ \\
&\quad + ce^{i\omega_p t}I_+N'_z - (s/2)e^{i(\omega_p-\omega_e)t}I_+N'_-\} + \mathrm{HC} \\
&\quad - \frac{3\alpha}{4} \sqrt{\frac{32\pi}{15}}\, Y_{2,-2}(\theta(t), \phi(t))\{e^{i(\omega_p+\omega_n+\omega_e)t}((c+1)/2)I_+N'_+ \\
&\qquad + se^{i(\omega_p+\omega_n)t}I_+N'_z + ((c-1)/2)e^{i(\omega_p+\omega_n-\omega_e)t}I_+N'_-\} + \mathrm{HC}. \qquad [12]
\end{aligned}$$

Again, HC indicates the Hermitian conjugate of the previous term. For the $Y_{2,-1}$ and $Y_{2,-2}$ terms, the Hermitian conjugation is to be taken for the entire previous bracketed term. As expected, the laboratory spin operators are rotated into linear combinations of operators native to the doubly rotating frame. The latter operators are indicated by primes. To reduce the complexity of the above Eq. [12], we have used s and c in place of sin β and cos β, respectively.

Macroscopic rate equations and $T^{X}_{1\rho}$. The form of the Hamiltonian in the doubly rotating frame given by Eq. [12] along with the spin density operator $\sigma(t)$ allows us to write a rate equation for the decay of magnetization along $\mathbf{B}_{\mathrm{eff}}$. All information concerning the ensemble of ^{1}H–^{15}N spins can be obtained from $\sigma(t)$. The macroscopic value for any observable, M, is given by the ensemble-averaged expectation value of its associated quantum operator. This average is given by the well-known trace relation

$$\langle M\rangle(t) = \mathrm{Tr}\{\sigma(t)M\}. \qquad [13]$$

We use $\langle M\rangle$ to indicate the macroscopic variable and M to indicate the quantum mechanical operator.

The equation of motion for $\sigma(t)$ in the doubly rotating frame (interaction frame) is governed by $V'(t)$ and is written as

$$\frac{d\sigma}{dt} = -\int_0^{\infty} (\langle [V'(t), [V'(t-\tau), \sigma(t) - \sigma^{\mathrm{eq}}]]\rangle)d\tau. \qquad [14]$$

The angled brackets ($\langle\ \rangle$) indicate that an ensemble average is to be taken over the time-dependent parts of $V'(t)$; σ^{eq} is the density operator at thermodynamic equilibrium. If we insert the expression for $V'(t)$ into the equation of motion given in Eq. [14], we then obtain

$$\frac{d\sigma}{dt} = -\frac{1}{2}\sum_{(q=-M,p=-m)}^{(M,m)} (J^{(q)}(\omega_p^{(q)})[A_p^{(-q)}, [A_p^{(q)}, \sigma(t) - \sigma^{eq}]]) \qquad [15]$$

The $J^{(q)}(\omega_p^{(q)})$ terms are spectral density functions sampled at the transition frequencies $\omega_p^{(q)}$; they arise from the aforementioned ensemble average over $V'(t)$ (vide infra). It is understood that in arriving at Eq. [15], we consider only those times t that are significantly longer than the correlation times characterizing the stochastic processes associated with $V'(t)$. This is a fundamental restriction of the semiclassical relaxation theory (*4, 11*). If we take the overall molecular tumbling as the stochastic process, then Eq. [15] is valid for times $t \gg \tau_m$, where τ_m is the molecular tumbling correlation time.

Eq. [13] gives the time behavior for $\langle M \rangle$, where $\langle M \rangle$ is the observed value for operator M. It seems to require prior integration of density operator Eq. [15]. Fortunately, this is not necessary since the operator methods of Abragam (*4*) allow us to derive the rate equation for M directly. One multiplies the density operator Eq. [15] by the desired observable M and then takes the trace. Using the fact that the trace of any product of operators is unchanged by a cyclic shuffle of the operators, one immediately obtains the macroscopic rate equation

$$\frac{d\langle M \rangle}{dt} = -\frac{1}{2}\sum_{(p,q)}^{(M,m)} (J^{(q)}(\omega_p^{(q)})\mathrm{Tr}\{[A_p^{(-q)}, [A_p^{(q)}, M]](\sigma(t) - \sigma^{eq})\}). \qquad [16]$$

Here, we need to define only the spectral densities $J^{(q)}(\omega_p^{(q)})$ and the double commutator, $[A_p^{(-q)}, [A_p^q, M]]$, which involves the observable of interest and the spin operators of $V'(t)$. The summation is over all terms in the transformed Hamiltonian $V'(t)$ given in Eq. [12]. Index q runs from $-M$ to M as in Eq. [4]. Recall that in going from the laboratory frame to the doubly rotating frame, the operators $A^{(q)}$ are mapped into linear combinations of operators $A_p^{(q)}$. The index p runs over the operators in these linear combinations.

The spectral densities $J^{(q)}(\omega_p^{(q)})$ are the Fourier transforms of the autocorrelation function for the various angular functions $F^{(q)}(\theta(t), \phi(t))$, evaluated at the frequencies $\omega_p^{(q)}$. Thus, for arbitrary frequency ω, we have

$$J^{(q)}(\omega) = \int_{-\infty}^{+\infty} (e^{(-i\omega t)}\langle F^{(q)}(\Omega_0)F^{*(q)}(\Omega(t))\rangle dt), \qquad [17]$$

where Ω stands for the angles (θ, ϕ). $\langle F^{(q)}(\Omega_0)F^{*(q)}(\Omega(t))\rangle$ is the autocorrelation function for a given $F^{(q)}(\theta(t), \phi(t))$ and is the direct result of the ensemble average in Eq. [14]. $J^{(q)}(\omega)$ is a real, even function of ω. An analytical form for $J^{(q)}(\omega)$ requires a motional model for the ^{15}N–^{1}H bond vector $\mathbf{r}_{np}$. Only then can the autocorrelation for the $F^{(q)}$ be described and the Fourier transform given by Eq. [17] evaluated. For example, the traditional model of the molecule as an isotropically tumbling rigid body yields

$$J^{(q)}(\omega) = \frac{|C^{(q)}|^2}{2\pi} \frac{\tau_m}{(1 + (\omega\tau_m)^2)}, \qquad [18a]$$

where τ_m is the molecular rotational correlation time. Note that the only q dependence is via the real constant $C^{(q)}$. The functional dependence on ω is independent of q. We hereafter refer to this functional dependence simply as $J(\omega)$. Equation [18a] can then be rewritten as

$$J^{(q)}(\omega) = \frac{|C^{(q)}|^2}{2\pi} J(\omega). \qquad [18b]$$

Physically, $J(\omega)$ represents the frequency distribution of the reorientational motions of the bond vector $\mathbf{r}_{np}$. The goal of the molecular dynamicist, then, is to characterize $J(\omega)$.

For an analysis of $T_{1\rho}^X$, the relevant observable is the spin operator N_z'. Therefore, we set $M = N_z'$ in Eq. [16]. After using the explicit $V'(t)$ terms shown in Eq. [12] to evaluate the double commutators and take their traces, we find that

$$\frac{d\langle N_z'\rangle}{dt} = -\frac{1}{T_{1\rho}^X}\langle N_z' - N_z'^0\rangle - \sigma_\rho^{HX}\langle I_z - I_z^0\rangle,$$

where

$$\begin{aligned}\frac{1}{T_{1\rho}^X} = \frac{3\alpha^2\hbar^4}{10}\Big\{&\frac{2}{3}\sin^2(\beta)J(\omega_e) + \frac{1}{3}[(\sin^4(\beta/2)J(\omega_p - \omega_n + \omega_e)\\ &+ \cos^4(\beta/2)J(\omega_p - \omega_n - \omega_e)]\\ &+ \cos^4(\beta/2)J(\omega_n + \omega_e) + \sin^4(\beta/2)J(\omega_n - \omega_e)\\ &+ \frac{1}{2}\sin^2(\beta)(J(\omega_p + \omega_e) + J(\omega_p - \omega_e))\\ &+ 2[\cos^4(\beta/2)J(\omega_p + \omega_n + \omega_e) + \sin^4(\beta/2)J(\omega_p + \omega_n - \omega_e)]\Big\}\end{aligned}$$

and

$$\begin{aligned}\sigma_\rho^{HX} = \frac{3\alpha^2\hbar^4}{10}\Big\{&\frac{1}{3}[(\sin^4(\beta/2)J(\omega_p - \omega_n + \omega_e) - \cos^4(\beta/2)J(\omega_p - \omega_n - \omega_e)]\\ &+ \frac{1}{2}\sin^2(\beta)(J(\omega_p + \omega_e) - J(\omega_p - \omega_e))\\ &+ 2[\cos^4(\beta/2)J(\omega_p + \omega_n + \omega_e) - \sin^4(\beta/2)J(\omega_p + \omega_n - \omega_e)]\Big\}. \qquad [19]\end{aligned}$$

Rigorously, ω_n should be replaced by the actual ^{15}N carrier frequency, ω (see Eq. [4]). However, ω differs from ω_n by less than a percent (of ω_n) as β varies from 1° to 90°. Thus, little error is introduced by using ω_n for arbitrary tip angle β. $\langle N_z'^0\rangle$ and $\langle I_z^0\rangle$ are the equilibrium magnetizations for nitrogens in the doubly rotating frame and protons in the lab frame, respectively; σ_ρ^{HX} represents the nitrogen–proton cross re-

laxation and is not to be confused with the spin density matrix $\sigma(t)$ discussed previously. Since Eq. [19] involves both $\langle N'_z - N'^0_z \rangle$ and $\langle I_z - I^0_z \rangle$, $\langle N'_z \rangle$ can generally change due to energy transfer to the lattice via $T^X_{1\rho}$, or due to cross relaxation to the protons via σ^{HX}_ρ. We note some distinctive features of the time constants $T^X_{1\rho}$ and σ^{HX}_ρ. First, their dependence on the spectral density functions, $J(\omega)$, is weighted by various trigonometric functions of the tip angle β. Additionally, the frequencies sampled by the spectral densities are ω_e, $\omega_p \pm \omega_e$, $\omega_n \pm \omega_e$, and $\omega_p \pm \omega_n \pm \omega_e$. These are sidebands of the usual sampling frequencies 0, ω_p, ω_n, and $\omega_p \pm \omega_n$ seen in the well-known expressions for T^X_1 and T^X_2. The fact that $T^X_{1\rho}$ samples different frequencies means that we can monitor different spectral regions of $J(\omega)$. This is shown schematically in Fig. 3. In principle, spin-lock sequences can be engineered to monitor $J(\omega)$ at a desired set of frequencies.

If the molecule suffers no motion other than rigid isotropic tumbling, the autocorrelation function for the reorientation of the internuclear vector $\mathbf{r}_{np}$ can be described by a single exponential with a decay constant τ_m. This results in a Lorentzian form for $J(\omega)$ shown in Eq. [18a]. Then for certain values of the flip angle β, $T^X_{1\rho}$ reduces to the familiar heteronuclear T^X_1 and T^X_2. Consider the limit where β approaches 0. This corresponds to a totally off-resonance RF field. Then all sine terms in Eq. [19] vanish. Typically, $(\omega_e/2\pi)$ is in the kilohertz range, as opposed to the megahertz values of Larmor frequencies $(\omega_n/2\pi)$ and $(\omega_p/2\pi)$. In such cases, we can neglect the RF contribution to the Larmor frequencies and make the approximations $J(\omega_p \pm \omega_n \pm \omega_e) = J(\omega_p \pm \omega_n)$, $J(\omega_p \pm \omega_e) = J(\omega_p)$, and $J(\omega_n \pm \omega_e) = J(\omega_n)$. We then arrive at the familiar T^X_1 expression

$$\lim_{\beta \to 0} \frac{1}{T^X_{1\rho}} = \frac{\alpha^2 \hbar^4}{10} \{J(\omega_p - \omega_n) + 3J(\omega_n) + 6J(\omega_p + \omega_n)\}, \qquad [20a]$$

$$\lim_{\beta \to 0} \sigma^{HX}_\rho = \frac{\alpha^2 \hbar^4}{10} \{6J(\omega_p + \omega_n) - J(\omega_p - \omega_n)\}. \qquad [20b]$$

Note that σ^{HX}_ρ reduces to the familiar cross-relaxation rate first derived by Solomon (*13*), and the rate equation [19] simply becomes one of the Solomon equations.

Now consider the limit where β approaches $(\pi/2)$ and therefore $\cos(\beta/2) = \sin(\beta/2) = \sqrt{2}/2$. This corresponds to the on-resonance limit. If we keep the approximations of $J(\omega_p \pm \omega_n \pm \omega_e) = J(\omega_p \pm \omega_n)$, $J(\omega_p \pm \omega_e) = J(\omega_p)$, and $J(\omega_n \pm \omega_e) = J(\omega_n)$ we get

$$\lim_{\beta \to \pi/2} \frac{1}{T^X_{1\rho}} = \frac{\alpha^2 \hbar^4}{20} \{4J(\omega_e) + J(\omega_p - \omega_n) + 3J(\omega_n) + 6J(\omega_p) + 6J(\omega_p + \omega_n)\}, \qquad [21a]$$

$$\lim_{\beta \to \pi/2} \sigma^{HX}_\rho = 0. \qquad [21b]$$

This is identical to the expression for T^X_2 except for the lowest-frequency term, which is $J(\omega_e)$ instead of $J(0)$. In principle, it should be possible to map the spectral density function near the zero frequency by measuring on-resonance $T^X_{1\rho}$ values for varying ω_e values. Note also that the cross-relaxation term vanishes. Therefore, the use of polarization-transfer methods from protons to nitrogens (X nuclei), which equalizes

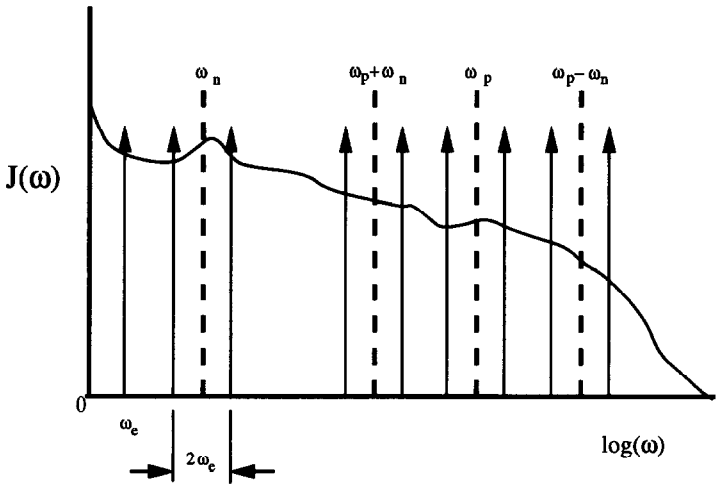

FIG. 3. Sampling of a hypothetical spectral density function $J(\omega)$ by $T_{1\rho}^{X}$. The arrowed spikes are the sampling frequencies. They are sidebands symmetrically offset by $\pm\omega_e$ to the usual sampling frequencies indicated by the dashed lines. The samplings are weighted by trigonometric functions of the $\mathbf{B}_{eff}$ tip angle, β.

the proton populations, is justified in the relaxation experiment discussed (see Fig. 5). For $\omega_e/2\pi$ in the kilohertz range, $J(\omega_e)$ will be sensitive to processes with correlation times much longer than those germane to the spectral density functions evaluated at the various Larmor frequencies $\omega_p \pm \omega_n$, ω_p, and ω_n. For protein molecules with τ_m in the range of nanoseconds, $\omega_e\tau_m \ll 1$. As a result, $J(\omega_e)$ is well approximated by $J(0)$. Therefore, in the limit of a weak on-resonance spin lock and the assumption of a Lorentzian spectral density function, $T_{1\rho}^{X}$ contains the same spectral information as T_2^X.

It is also informative to compare the behavior of these relaxation times as a function of τ_m with the assumption that $J(\omega)$ is Lorentzian. Figure 4 plots $\log_{10}(T_i)$ against $\log_{10}(\tau_m)$, where T_i is either $T_{1\rho}^{X}$ at various flip angles β, T_1^X, or T_2^X. We note that $T_{1\rho}^{X}$ for $\beta = 90°$ shows the same kind of behavior as T_1^X. Specifically, both relaxation times ultimately increase with correlation time after reaching a minimum. This increase occurs for $\tau_m > (1/\omega_{min})$, where ω_{min} represents the lowest-frequency spin transition for a particular relaxation time. Essentially, slower molecular tumbling results in longer τ_m values, which weight the spectral density function toward lower frequencies. This is easily visualized if $J(\omega)$ is a simple Lorentzian distribution; a longer τ_m produces a sharper, narrower "peak" about zero frequency. As a result, the overlap between the high-intensity portion of $J(\omega)$ and the nonzero spin transition frequencies progressively decreases. The associated relaxation process is therefore retarded and the relaxation time lengthens. Since the lowest transition frequency sampled by $T_{1\rho}^{X}$ is typically several orders of magnitude lower than that in T_1^X, the increasing edge of $T_{1\rho}^{X}$ occurs at much longer correlation times. Clearly, τ_m can never exceed $1/\omega_{min}$ for T_2^X. Therefore, T_2^X continues to decrease monotonically with τ_m until plateauing at a particular rigid lattice value (not shown). Note again that for τ_m on the order of nanoseconds, T_2^X and $T_{1\rho}^{X}$ for $\beta = 90°$ are equal. However, it must be stressed that

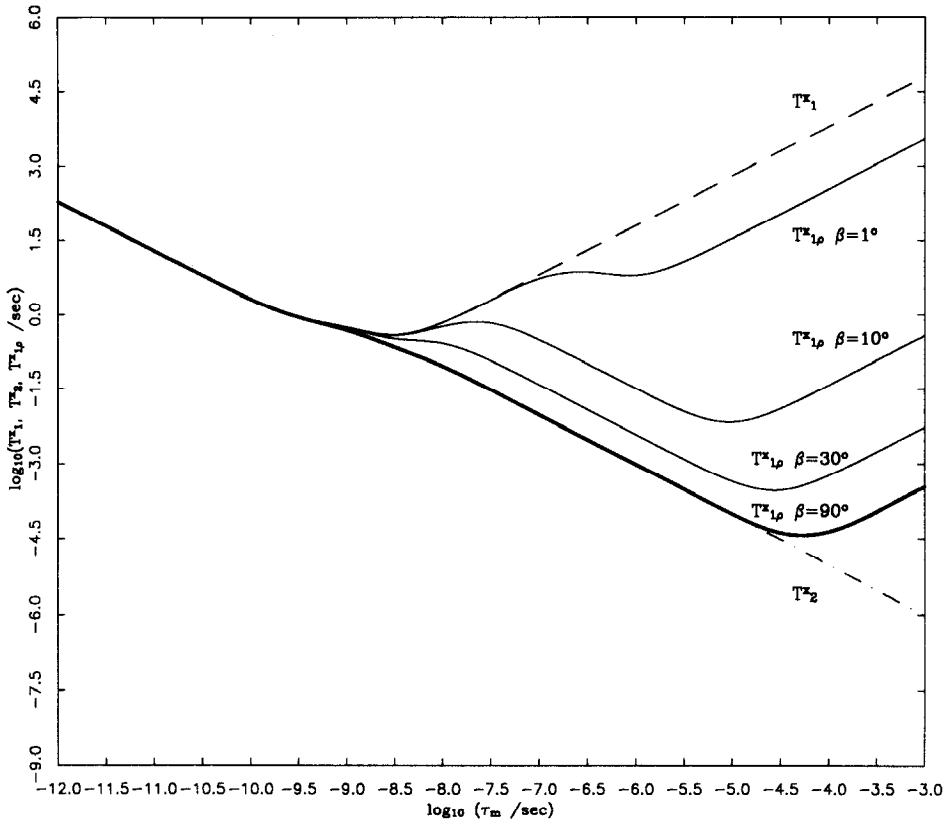

FIG. 4. Log_{10}–$\log_{10}$ plot of T_1^X, T_2^X, and $T_{1\rho}^X$ versus molecular correlation time τ_m. $T_{1\rho}^X$ is shown for flip angles β = 90°, 30°, 10°, and 1°. The $T_{1\rho}^X$ plots are indicated by the solid curves with flip angle labels. The T_1^X and T_2^X plots are shown by the broken curves above and below, respectively.

this equality holds only if the spectral density function $J(\omega)$ is given by a Lorentzian (and only then is τ_m defined). Figure 4 also shows the behavior of $T_{1\rho}^X$ as a function of τ_m at flip angle values of β = 1°, 10°, and 30°. As β progresses from 0° to 90°, we see the transition from T_1^X to T_2^X behavior. Note that since Fig. 4 is plotted on a logarithmic scale, the T_1^X and $T_{1\rho}^X$ values for τ_m in the range of 3–4 ns may appear deceptively close. In fact, for τ_m = 3.5 ns, $T_1^X/T_{1\rho}^X$ is approximately 2.

EXPERIMENTS AND RESULTS

The 2D NMR pulse sequence for measuring $T_{1\rho}^X$ values is shown in Fig. 5. The sequence allows the measurement of $T_{1\rho}^X$ times for each X nucleus in a molecule. In our experiments, the X nuclei are protein backbone amide ^{15}N nuclei. The sequence begins with equilibrium proton magnetization which is transferred via an INEPT sequence to the nitrogens. After the INEPT transfer, we have antiphase $2I_zN_y$ magnetization. We follow with a tuned refocusing period to get N_x magnetization. A ^{15}N spin lock keeps the N_x magnetization locked along x for a relaxation delay τ. The remnant magnetization is then frequency labeled during the t_1 evolution period. A reversed, refocused INEPT converts the magnetization back to the protons for sen-

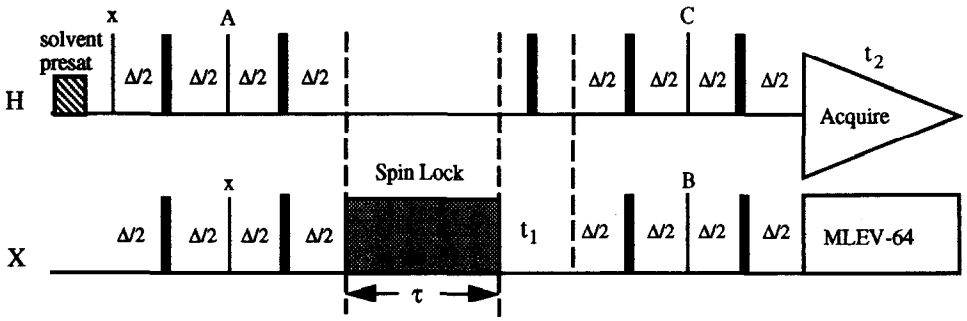

FIG. 5. Two-dimensional pulse sequence for measuring $T_{1\rho}^{X}$ times in heteronuclear HX systems. Proton (^{1}H) pulses are shown on the upper trace and X nuclei pulses are given on the lower trace. Solvent suppression is achieved by initial presaturation of the solvent protons; 90° and 180° pulses are indicated by the thin and thick vertical bars, respectively. Delays include the X-nucleus spin lock, which is indicated by the shaded region of length τ, the tuned delay $\Delta/2 = 1/(4J_{HX})$, the X nucleus evolution period t_1, and the proton detection period t_2. The pulse phases are as follows: (A) $y, -y \ldots$, (B) $x, x, -x, -x, \ldots$, + TPPI, (C) $x, x, x, x, -x, -x, -x, -x, \ldots$. The receiver phases are $-x, x, x, -x, x, -x, -x, x, \ldots$. Broadband decoupling is used during the proton detection period as indicated by the MLEV-64 period on the X nuclei.

sitivity-enhanced, broadband-decoupled acquisition. Sign discrimination in F_1 is achieved by the TPPI method of Marion and Wüthrich (*14*). The minimum phase cycle involves eight scans, typically with 256 t_1 blocks acquired. The final result is a heteronuclear COSY spectrum with the cross-peak intensities attenuated by the extent of relaxation allowed. A typical spectrum is shown in Fig. 6. Each cross peak corresponds to the backbone amide ^{15}N of a specific residue. In our experiments, the ^{15}N spin lock was composed of contiguous ^{15}N 180°_{x} pulses. Use of other pulse trains such as WALTZ-16 was avoided since the magnetization is not necessarily fixed along $\mathbf{B}_{eff}$ during these sequences. The 180° pulse lengths were 168 μs, corresponding to $\omega_1/2\pi = 2976$ Hz. The tip angles (β) for the amides ranged between 75° and 90°. Thus we can approximate the spin lock as being on resonance for all backbone amide cross peaks.

We have implemented this experiment on a General Electric Ω500 spectrometer and applied it to the 100% ^{15}N-enriched protein eglin c. Eglin c functions as an inhibitor for proteinases such as elastase, subtilisin, and chymotrypsin. It consists of 70 residues resulting in a molecular weight of 8111 Da. The proton assignments have been given by Hyberts *et al.* (*15*). The sample concentration was ≈4.5 mM and the pH was set to 3.0. For a series of nine 2D spectra, the total acquisition time was approximately two days. Relative peak intensities were obtained by integrating slices along the F_2 dimension through the cross-peak maxima for each 2D spectrum. For each cross peak, the intensities were fitted to a monoexponential decay by a nonlinear least-squares fit routine using the software package PLOT (New Unit Inc., Ithaca, New York). The fitted decay constant gives $T_{1\rho}^{X}$. An example is shown in Fig. 7.

The distribution of $T_{1\rho}^{X}$ versus residue number is shown in Fig. 8. Blank columns indicate either prolines or residues that could not be quantitated due to resonance overlap. Data at the positions 71–74 indicate the 4 arginine side-chain ϵ-nitrogens for the residues Arg 22, 48, 51, and 53, which also constitute HX spin systems. The values are uniform for the backbone nitrogens of the protein core. The average $T_{1\rho}^{X}$ value is 215 ms with an uncertainty of ±11 ms. This is approximately half of the average

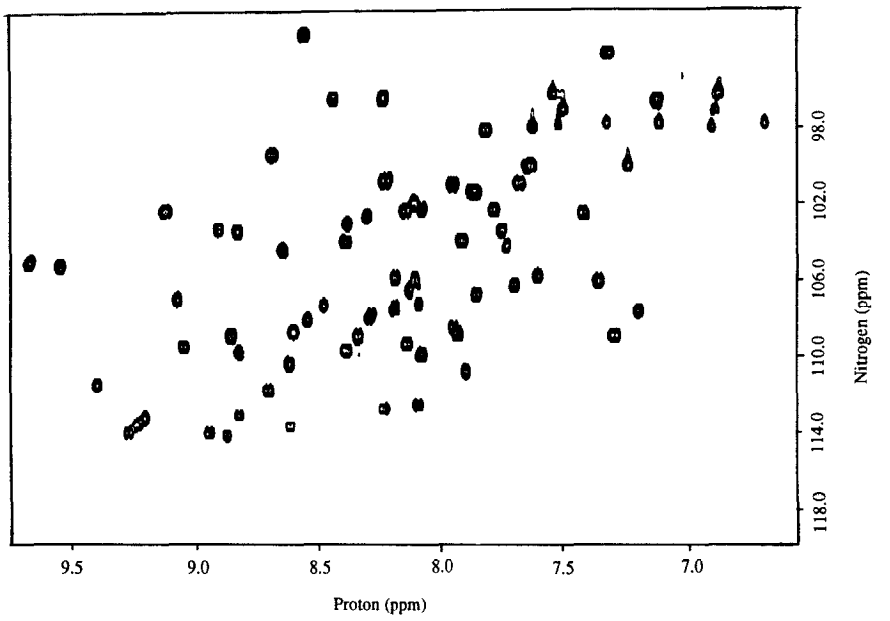

FIG. 6. Typical spectrum from the pulse sequence shown in Fig. 5 as applied to the protein eglin c. The data matrix consists of 256 t_1 blocks of 2048 complex points each. The data were processed by FTNMR (Hare Research Inc.) on a Sun 3/260. The proton (F_2) dimension was strip transformed and zero-filled twice, whereas the ^{15}N (F_1) dimension was zero-filled once. The ^{15}N axis was referenced arbitrarily by setting Val 63 to 114 ppm. Window functions included 45° shifted sine bells in both dimensions. The spin lock consisted of contiguous 180° ^{15}N pulses with $\omega_1 \approx 3$ kHz.

T_1^X for the protein core. A 2 to 1 ratio of T_1^X to $T_{1\rho}^X$ is consistent with a $\tau_m \approx 3.5$ ns in Fig. 4, where a factor of 2 translates into a $\log_{10}$ value ≈ 0.3. The values for $T_{1\rho}^X$ are significantly longer for the residues of the N-terminus (residues 1–8) and those of the protease binding loop (residues 42–47). For example, Gly 4 and Glu 6 have $T_{1\rho}^X$ values of 526 and 413 ms while binding loop residues Leu 45 and Asp 46 have $T_{1\rho}^X$ values of 313 and 346 ms. The arginine side chains show significantly longer $T_{1\rho}^X$ values as well. Arg 22 and Arg 48, which are located on the surface of the protein, have longer $T_{1\rho}^X$ values than Arg 51 and Arg 53, which lie in the protein interior and are involved in many intramolecular hydrogen bonds (*16–18*). The data corroborate results from both the ^{15}N T_1^X and NOE^X measurements, which showed significant deviations for these regions of the molecule. Together, they provide strong evidence that the N-terminus and binding loop experience greater conformational mobility than the rest of the protein. Motional analyses which use a Lorentzian form for $J(\omega)$ produce a molecular correlation time of 3.5 ± 0.2 ns. Since our approximately on-resonance spin lock had $\gamma B_1/2\pi \approx 3$ kHz, we are in the limit that $\omega_e \tau_m \ll 1$. Then, $T_{1\rho}^X$ should be indistinguishable from T_2^X provided $J(\omega)$ is a Lorentzian distribution.

We have performed ^{15}N T_2^X measurements on eglin c and compared them to the corresponding $T_{1\rho}^X$ values. Interestingly, the T_2^X values are uniformly lower than the $T_{1\rho}^X$ values for *all* residues. The T_2^X values were determined by two methods. The first replaces the spin lock in the $T_{1\rho}^X$ experiment by a single ^{15}N 180° pulse at the center of relaxation delay, τ. The second method uses a Carr–Purcell–Meiboom–Gill (CPMG)

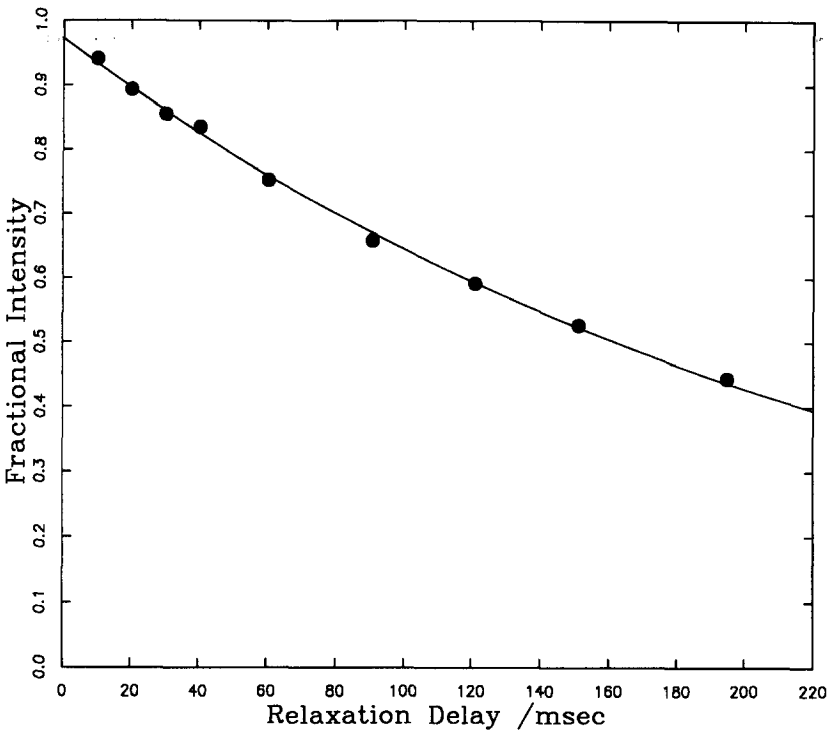

FIG. 7. Example of ^{15}N $T_{1\rho}^{X}$ fit for the His 65 residue in eglin c. The $T_{1\rho}^{X}$ value is 237 ms with an rmsd of 2.2%.

train of refocusing ^{15}N 180° pulses. CPMG duty cycles of 1 and 2% were used, with the ^{15}N 180° pulse width being 110 μs. These approaches are shown in Fig. 9. The resultant T_2^X values are $\approx$50 and 25% reduced from the $T_{1\rho}^{X}$ values for the single refocusing pulse and CPMG train (1% duty cycle), respectively. A comparison of relaxation curves for the three methods for residue His 65 of eglin c is shown in Fig. 10. The discrepancies from the $T_{1\rho}^{X}$ values are well outside the range of uncertainty for both the $T_{1\rho}^{X}$ and the T_2^X experiments. It should be stressed that the relaxation times for all residues in eglin c *increase* without exception. In addition, the relative profile of relaxation times seen in Fig. 8 is essentially preserved; those ^{15} N spins that have relatively longer T_2^X times also have longer $T_{1\rho}^{X}$ times.

A rigorous explanation of why the $T_{1\rho}^{X}$ values are significantly longer than the corresponding T_2^X values remains elusive.[1] Chemical exchange due to conformational isomerizations of the protein can cause apparently shorter T_2^X values, especially in the single 180° experiment. However, such exchange processes should be localized in the protein and therefore cannot explain the global increase of $T_{1\rho}^{X}$ over T_2^X.

[1]*Note added in proof.* We have subsequently found that the short T_2^X values are caused by the evolution of in-phase $N_{x,y}$ magnetization into antiphase $2I_zN_{y,x}$ magnetization. Antiphase magnetization relaxes much faster than in-phase magnetization due to dipole–dipole interactions between the amide proton and other spatially close protons. Therefore, the short T_2^X values are caused by proton–proton dipolar relaxation and not scalar relaxation of the second kind.

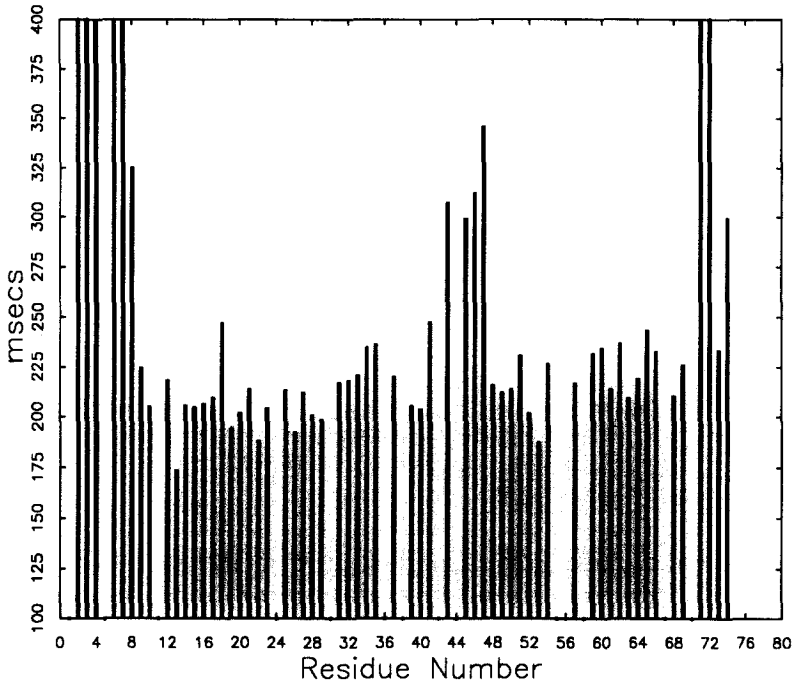

FIG. 8. Distribution of $T_{1\rho}^{X}$ for the ^{15}N nuclei in eglin c. Blank columns are due to either prolines or overlapped cross peaks. The average uncertainty in the $T_{1\rho}^{X}$ values is ±11 ms. Significantly larger $T_{1\rho}^{X}$ values are observed for the more mobile parts of the protein. $T_{1\rho}^{X}$ values for the first residues (e.g., 2–4, 6) exceed 500 ms and are off scale. Positions 71 to 74 are the N$^{\epsilon}$ of the arginines in positions 22, 48, 51, and 53. The N$^{\epsilon}$ at positions 22 and 48 are solvent exposed and have off-scale $T_{1\rho}^{X}$ values of 542 and 781 ms, respectively. In contrast, the N$^{\epsilon}$ at positions 51 and 53 are involved in intramolecular hydrogen bonding and have much shorter $T_{1\rho}^{X}$ values of 234 and 300 ms, respectively.

Scalar relaxation of the second kind (*4*) has been suggested by Kay *et al.* (*3*) as the culprit mechanism causing the short T_2^X values. This mechanism would involve fluctuations of the scalar interaction between the ^{15}N and ^{1}H caused by zero-quantum transitions between the amide protons and neighboring protons. The $T_{1\rho}^{X}$ experiment would be immune to the effects of scalar relaxation, since it decouples the ^{15}N nuclei from their amide protons during the spin lock. In contrast, the J_{NH} coupling remains intact in the single 180° experiment (and to a lesser extent in the CPMG experiment) and thus the scalar relaxation would result in apparently shorter T_2^X times. However, this explanation seems unlikely for reasons discussed by Abragam (*4*). In particular, scalar relaxation of the second kind demands that the amide protons have relaxation times much shorter than $(2\pi J_{NH})^{-1}$. (J_{NH} is approximately 90 Hz, and therefore $1/2\pi J_{NH}$ is approximately 1.77 ms/rad). If this were the case, heteronuclear decoupling for the ^{15}N evolution would be unnecessary since the ^{15}N doublet corresponding to populations with the amide proton spin up and spin down would automatically collapse. Furthermore, the theory of the proposed scalar relaxation treats the amide protons as lattice variables instead of spin operators. This means that the amide proton relaxation must occur faster than any time interval relevant to the ^{15}N relaxation experi-

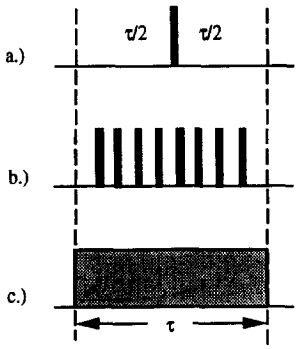

FIG. 9. Alternative methods of measuring transverse relaxation times, T_2^X. (a) Single 180° refocusing pulse; (b) CPMG 180° pulse train. (c) Spin lock. These sequences can all be inserted just prior to the t_1 evolution period in Fig. 5. The transverse relaxation times are the shortest for the single 180° pulse. They are progressively longer for CPMG trains of a larger duty cycle. In the limit that the duty cycle reaches 100% we get an on-resonance spin lock in case (c).

ments. In effect, the amide proton spin flips act as another stochastic perturbation from the lattice on the ^{15}N spins, and the amide proton T_1 and T_2 become additional correlation times describing the "random field" seen by the ^{15}N spins. However, the proton relaxation times are at least in the 100 ms time scale. Clearly then, the amide protons cannot be considered part of the lattice and an explanation using the theory for scalar relaxation of the second kind (*4*) is inappropriate.

An alternative explanation does not involve scalar relaxation at all, but rather the spectral density function, $J(\omega)$. Recall that the equivalence between T_2^X and $T_{1\rho}^X$ is

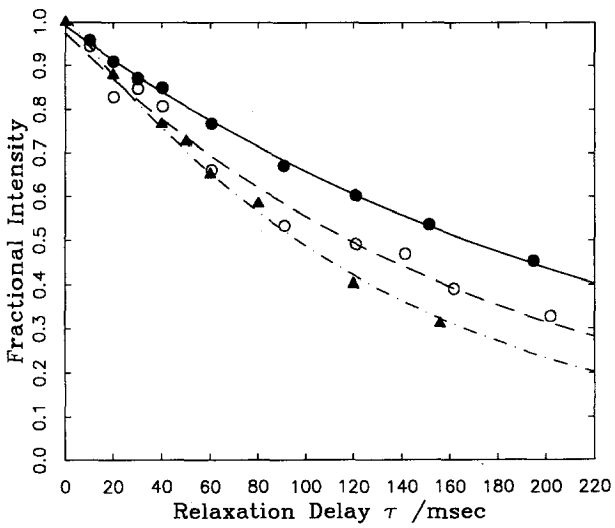

FIG. 10. Comparison of T_2^X via single 180°, T_2^X via CPMG, and $T_{1\rho}^X$ for the same ^{15}N nucleus (His 65). The triangular plot is from the single 180° experiment, the open circle plot is from the CPMG experiment, and the solid circle plot is from the $T_{1\rho}^X$ experiment of Fig. 5. The relaxation times are 136 ± 4, 177 ± 9, and 237 ± 4 ms, respectively.

based on the approximation that $J(\omega_e) = J(0)$. This approximation assumes that $J(\omega)$ is a Lorentzian described by a single correlation time, τ_m, which is on the order of nanoseconds. In this case, $J(\omega)$ does not vary significantly over the low (kilohertz) frequencies characteristic of typical $(\omega_e/2\pi)$ values, and therefore the approximation is justified. However, there is no a priori reason to expect such flat behavior of $J(\omega)$ at low frequencies. There may be internal protein motions at such frequencies that lead to much more complex spectral densities. It is therefore possible that $J(\omega_e)$ is significantly different from $J(0)$, and that this alone accounts for the different results from the $T_{1\rho}^X$ experiment and the other transverse relaxation experiments.

CONCLUDING REMARKS

We have shown theoretically that heteronuclear $T_{1\rho}^X$ measurements can offer spectral information not available in either T_1^X, T_2^X, or NOE^X. Specifically, $T_{1\rho}^X$ samples sideband frequencies offset by $\pm\omega_e$ from the zero-, single-, and double-quantum frequencies usually sampled in an HX spin system. When a Lorentzian form for $J(\omega)$ is assumed, $T_{1\rho}^X$ reduces to T_1^X and T_2^X for the following cases. In the limit of a vanishing spin-lock field, $T_{1\rho}^X$ becomes T_1^X, and the rate equations for relaxation become Solomon's equations (*13*). In the limit of an on-resonance spin lock, $T_{1\rho}^X$ resembles T_2^X except that the lowest frequency sampled is the effective field frequency, ω_e. If ω_e is much smaller than $1/\tau_m$, then $T_{1\rho}^X$ contains the same spectral information as T_2^X.

We have also presented a 2D heteronuclear pulse sequence to measure site-specific $T_{1\rho}^X$ values in biomolecules. We have applied the $T_{1\rho}^X$ experiment to the 70-residue protein, eglin c. The $T_{1\rho}^X$ values are significantly longer than the corresponding T_2^X values obtained by using a single 180° pulse in the center of the relaxation delay, or by using a CPMG pulse train. Furthermore, we have observed that the $T_{1\rho}^X$ values are longer for all ^{15}N nuclei in the protein. Therefore, the lengthening cannot be attributed to chemical exchange due to conformational isomerizations. Additionally, the lengthening cannot be attributed to scalar relaxation of the second kind (*4*), which demands proton relaxation times well below the millisecond time scale. Those interested in a quantitative analysis of their data should consider carefully how the transverse relaxation times are to be measured. The variation of $T_{1\rho}^X$ values along the backbone of eglin c shows that it is sensitive to dynamical heterogeneity. $T_{1\rho}^X$ is therefore another useful parameter in the experimental characterization of biomolecular motions.

ACKNOWLEDGMENTS

We thank Dr. Dirk Heinz and Dr. Marcus Grütter, Ciba-Geigy, Basel, Switzerland, for the gift of ^{15}N eglin c. We also thank Dr. Marc Adler for useful discussions and assistance with the use of PLOT. This work was supported by NSF Grants DMB-8616059, DMB-9007878, and BBS 8615223 and NIH Training Grant T32-GM08270-03 to J.P.

REFERENCES

1. (*a*) N. R. NIRMALA AND G. WAGNER, *J. Am. Chem. Soc.* **110,** 7557 (1988); (*b*), *J. Magn. Reson.* **82,** 659 (1989).
2. M. J. DELLWO AND A. J. WAND, *J. Am. Chem. Soc.* **111,** 4571 (1989).
3. L. E. KAY, D. A. TORCHIA, AND A. BAX, *Biochemistry* **28,** 8972 (1989).
4. A. ABRAGAM, "The Principles of Nuclear Magnetism," Chap. 8, Clarendon Press, Oxford, 1961.

5. G. P. JONES, *Phys. Rev.* **148,** 332 (1966).
6. T. L. JAMES, G. B. MATSON, AND I. D. KUNTZ, *J. Am. Chem. Soc.* **100,** 3590 (1978).
7. T. L. JAMES AND G. B. MATSON, *J. Magn. Reson.* **33,** 345 (1979).
8. T. L. JAMES, G. B. MATSON, I. D. KUNTZ, AND R. W. FISHER, *J. Magn. Reson.* **28,** 417 (1977).
9. T. L. JAMES AND S. P. SAWAN, *J. Am. Chem. Soc.* **101,** 7050 (1979).
10. (*a*) J. S. Blicharski, *Acta Phys. Pol. A* **41,** 223 (1972); (*b*) *Z. Naturforsch. A* **27,** 1355 (1972).
11. R. R. ERNST, G. BODENHAUSEN, AND A. WOKAUN, "Principles of Nuclear Magnetic Resonance in One and Two Dimensions," pp. 50–57, Clarendon Press, Oxford, 1987.
12. O. W. SØRENSEN, G. W. EICH, M. H. LEVITT, G. BODENHAUSEN, AND R. R. ERNST, *Prog. NMR Spectrosc.* **16,** 163 (1983).
13. I. SOLOMON, *Phys. Rev.* **99,** 559 (1955).
14. D. MARION AND K. WÜTHRICH, *Biochem. Biophys. Res. Commun.* **113,** 967 (1983).
15. S. G. HYBERTS AND G. WAGNER, *Biochemistry* **29,** 1465 (1990).
16. (*a*) W. BODE, E. PAPAMOKOS, D. MUSIL, U. SEEMÜLLER, AND H. FRITZ, *EMBO J.* **5,** 813 (1986); (*b*) W. BODE, E. PAPAMOKOS, AND D. MUSIL, *Eur. J. Biochem.* **166,** 673 (1987).
17. C. A. MCPHALEN, A. SCHNEBLI, AND M. N. G. JAMES, *FEBS Lett.* **188,** 55 (1985).
18. C. A. MCPHALEN AND M. N. G. JAMES, *Biochemistry* **26,** 261 (1987).